

Harmonic Analysis of a Saturated Iron-Core Superconducting Fault Current Limiter using Jiles-Atherton Hysteresis Model

*D. Sarkar, *D. Roy, *A. B. Choudhury, **S. Yamada

*Indian Institute of Engineering Science and Technology, Shibpur,
Howrah- 711 103, West Bengal, India,

(debraj.sarkar25@gmail.com, dbr_roy@yahoo.co.in, ab_choudhury@yahoo.com)

**Institute of Nature and Environmental Technology (K-INET), Kanazawa University,
Kanazawa, Japan, (yamada@magstar.ec.t.kanazawa-u.ac.jp)

Abstract

Saturated iron core superconducting fault current limiters (SISFCL) has been the topic for research in recent years on both its experimental and theoretical aspects owing to its efficient fault limiting. Previously, mathematical models were developed using an approximated B-H curve. But since the working principle of the limiter requires changes in magnetic state of saturation and unsaturation, the inclusion of hysteresis in the model is essential. This paper presents a mathematical model of SISFCL using Jiles Atherton hysteresis model and its subsequent numerical solution. A comparison is made with the responses obtained considering B-H curve. Finite Element Method is also utilized to support the findings. Harmonic analysis has been carried out utilizing CWT and FFT on the circuit current response of FCL under normal and faulted conditions. The results obtained from CWT and FFT are compared and reported.

Key words

Hysteresis, J-A model, fault current limiter, saturated core, superconducting coil, SISFCL, CWT, FFT.

1. Introduction

The demand in electricity is increasing with the development of technology and general lifestyle. Power system capacity has been augmented to cope with the system demand which in turn increases the short circuit capacity. With the change in network size, the frequency of occurrence of faults also increases. Incidents of power failures, such as those in Auckland, New

Zealand (1998, 2006 and 2009), North America (2003), Malaysia (2005) and Sydney, Australia (2009), illustrate the vulnerability of modern power systems. This vulnerability is speculated to increase as the renewable energy sources are continually added to the system [1, 2]. This short circuit capacity may exceed the circuit breaker interrupting capacity. Avoiding the costly and laborious process of changing to new circuit breakers, the use of fault current limiters was imminent. In the recent years, the concepts of high temperature superconducting limiters have been receiving a lot of attention [3, 4]. The uses of this kind of limiters are slowly finding their way as reliable solution to vulnerability problems for the modern power systems [4, 5].

Saturated iron core superconducting fault current limiter (SISFCL) is gaining popularity than the other conventional current limiting method owing to the capability of the device in limiting the current and providing very low impedance during normal operation [6]. The SISFCL has found its way in both transmission and distribution applications due to its preferable and promising impedance characteristics. A successful installation and implementation is reported in [7, 8].

The SISFCL employs change in permeability of the core to perform the current limiting while maintaining low impedance during normal operation. For the complete understanding and the analysis of the system, a mathematical modelling needs to be formulated. Previous mathematical models [9-11] describes the SISFCL considering B-H curve of the core material. But as the performance of the SISFCL depends greatly on its ability to change its magnetic state of saturation to unsaturation and back, the inclusion of a hysteresis loop will be more realistic instead. In this paper, the author presents a novel mathematical model considering Jiles Atherton hysteresis model [12]. As a comparison, the output responses of the model, numerically solved in MATLAB, is compared to the responses of the limiter obtained considering a simpler B-H curve. The same comparisons are drawn from the output of FEM analysis in support to the previous analysis. Ansoft Maxwell software is used for this FEM solution. Lastly, a comparison is made for the two cases from the harmonic view point. Both Continuous Wavelet Transform (CWT) and Fast Fourier Transform (FFT) are employed in the harmonic analysis.

2. Working principle

The schematic model of the SISFCL is shown in Fig. 1. The DC coil in the centre provides necessary biasing to saturation in the ferromagnetic core. Two separate AC coils, placed on the extreme ends on the device, carry the load current. The AC coils are wound in opposite to each other. Hence, at any instant the flux produced from the AC coils will oppose the flux produced by

the DC coil in one core and support in the other. The biasing of the DC coil should be large enough to saturate the cores even in the presence of the opposing AC flux in the normal condition. In this condition, the permeability of the material at this field intensity is approximately equal to that of air making the impedance of the device nearly equal to that of an air core inductor. During fault, the increased circuit current, hence increased field intensity, oscillates with larger amplitude, de-saturating one of the cores. The other core reaches to a more saturated zone. De-saturation of the core yields a high permeability and the effective impedance of the device increases to high value to limit the fault current. After the fault clearance, the load current drops and the SISFCL regains the state of saturation again. Since the operation of the device depends on the change in permeability of the cores, the reaction time for limiting and recovery is almost immediate.

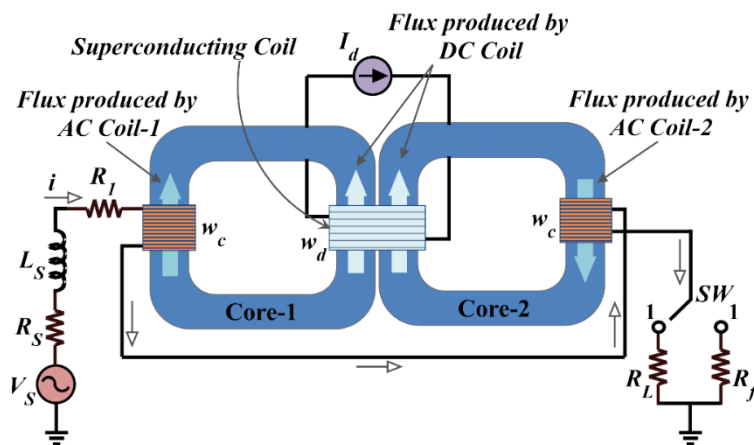


Fig.1. Schematic diagram of a SISFCL

3. Jiles Atherton Hysteresis model

As mentioned earlier, the mathematical model formulated previously was considering the B-H curve. But since hysteresis is a natural phenomenon observed in ferromagnetic materials, the inclusion of this phenomenon is necessary for the accurate analysis of the device. Several techniques of modelling hysteresis have been developed over the years, among which the Preisach's Model and the Jiles-Atherton's model [12] are more popular. In this paper the J-A model has been employed to study the transient behaviour of SISFCL.

The relation between the flux density and the magnetic field intensity is described by the well-known equation,

$$B = \mu H = \mu_0 \mu_r H = \mu_0 (H + M) \quad (1)$$

M in the equation refers to the magnetization or field intensity within the material that is developed by the magnetic domains. This relationship takes the form of a bi-stable sigmoid and is defined by the permeability (μ) of the material. If a magnetic material was able to return all of the magnetic energy that was input, the resulting magnetization curve would represent itself as of a single valued sigmoid. This curve, referred to as the anhysteretic magnetization curve, represents the ideal or lossless magnetization of a material. The mathematical representation is given in equation 2.

$$M_{an} = M_{sat} \left(\coth \left(\frac{H_e}{a} \right) - \frac{a}{H_e} \right) \quad (2)$$

According to the J-A model, the magnetization M is represented as the sum of the irreversible magnetization M_{irr} , due to domain wall displacement, and the reversible magnetization M_{rev} , due to domain wall bending.

$$M = M_{rev} + M_{irr} \quad (3)$$

Where M_{irr} is defined as,

$$\frac{dM_{irr}}{dH} = \frac{M_{an} - M_{irr}}{k\delta - \alpha(M_{an} - M_{irr})} \quad (4)$$

Where $\delta = \text{sign}(dH / dt)$ is a directional parameter, +1 for $\frac{dH}{dt} > 0$ and -1 for $\frac{dH}{dt} < 0$, k is parameter defining the pinning site density of domain walls. It is assumed to be the major contribution to hysteresis. The reversible magnetization is described as a component of difference of irreversible and anhysteretic magnetization,

$$M_{rev} = c(M_{an} - M_{irr}) \quad (5)$$

Where c is a domain flexing parameter, defining the amount of reversible magnetization due to wall bowing and reversal rotation, included in the magnetization process. Combining the above equations and rearranging the terms, the J-A model is described as,

$$\frac{dM}{dH} = \frac{(1-c) \frac{M_{an} - M}{\text{sign}\left(\frac{dH}{dt}\right) k(1-c) - \alpha(M_{an} - M)} + c \frac{dM_{an}}{dH_e}}{1 - \alpha c \frac{dM_{an}}{dH_e}} \quad (6)$$

The above equation provides the mathematical model of ferromagnetic hysteresis which is utilized in the model of the current limiter. In this paper, a sample core (Table 1) is considered for the analysis.

Table 1. J-A constants of the sample core

M_s			α	a
1.			1	1
7×10^6	.1	00	$\times 10^{-3}$	000

4. Mathematical model

The mathematical model is based on the schematic diagram in Fig. 1. The SISFCL is shown to be in series in between the voltage source (V_s) and the load (R_L) along with a fault resistance R_f . The fault is simulated by switching the load R_L to R_f . The source resistance and inductance is denoted by R_s and L_s respectively, whereas R_1 representing the total coil resistance. The variables w_d and w_c represent the number of turns of the DC and AC current carrying windings respectively. The mean magnetic path of each core and the DC biasing current is represented by l and I_d respectively. According to the Ampere's law, the following equations can be formulated for each of the two cores.

$$w_d I_d - w_c i = H_1 l \quad (7)$$

$$w_d I_d + w_c i = H_2 l \quad (8)$$

The subscripts 1 and 2 represent core 1 and core 2. After subsequent calculations, the induced voltage across the two coils is described as [10, 11],

$$u_1 = -e_1 = -\mu_0 w_c A \frac{dH_1}{dt} \left(1 + \frac{dM_1}{dH_1}\right) = L \frac{di}{dt} \left(1 + \frac{dM_1}{dH_1}\right) \quad (9)$$

$$u_2 = -e_2 = -\left(-\mu_0 w_c A \frac{d(H_2 + M_2)}{dt}\right) = L \frac{di}{dt} \left(1 + \frac{dM_2}{dH_2}\right) \quad (10)$$

Where $L = \frac{\mu_0 w_c^2 A}{l}$

Now following Kirchoff's law, the circuit equation is

$$V_o(t) = u_1 + u_2 + u_R + u_L = u_1 + u_2 + i(R_S + R_1 + R_L) + L_S \frac{di}{dt} \quad (11)$$

Substituting the above equations and rearranging, we obtain,

$$\frac{di}{dt} = \frac{V_o(t) - i(R_S + R_1 + R_L)}{L \left(2 + \frac{dM_1}{dH_1} + \frac{dM_2}{dH_2}\right) + L_S} \quad (12)$$

At the instant of fault the load resistance R_L is switched to R_f . The non-linear differential equation in circuit current i , following the other variables such as voltage across SISFCL and the DC coil, is solved using numerical method in MATLAB environment.

5. Simulation Results

Digital simulations were carried out with the values of the circuit parameter shown in Table 2. The model is simulated at 50 Hz for 0.06 seconds covering three cycles. Fig. 2 shows the transient response of the SISFCL for both normal and faulted condition. The fault is made to occur at 0.02s to have one cycle in normal and the other two in the faulted condition. The normal load resistance is taken as 3.4 ohm to have a 10 A circuit current in normal operation without the limiter. It can be observed that the presence of the FCL do not affect the normal current as it presents low impedance close to twice the value of an air core inductor [13]. To simulate a fault, the load resistance is changed to 0.34 ohm for a prospective fault current of 100A. The limiter can be observed to suppress this current to about 55A, thus achieving a 45 percent fault suppression. It should be noted here that the above explanations were for the case where hysteresis was considered in the mathematical model. The plot of voltage across the DC coil is shown in Fig. 3. The plot shows a very low value of voltage appears across the DC coil during normal operation and increases significantly during fault. This change in the voltage is due to the

rate of change in flux density (shown in Fig. 4). The flux density plot shows a very low variation during normal operation and it increases during fault due to the large AC flux interaction. This sudden increase in voltage across DC Coil is of great concern as it can lead to probable damage of the source [14]. The normal operating point is deliberately chosen close to the knee flux density, but still the variation in flux density in normal condition is low. This is a typical hysteresis phenomenon where the flux density does not change considerably with the change in field intensity.

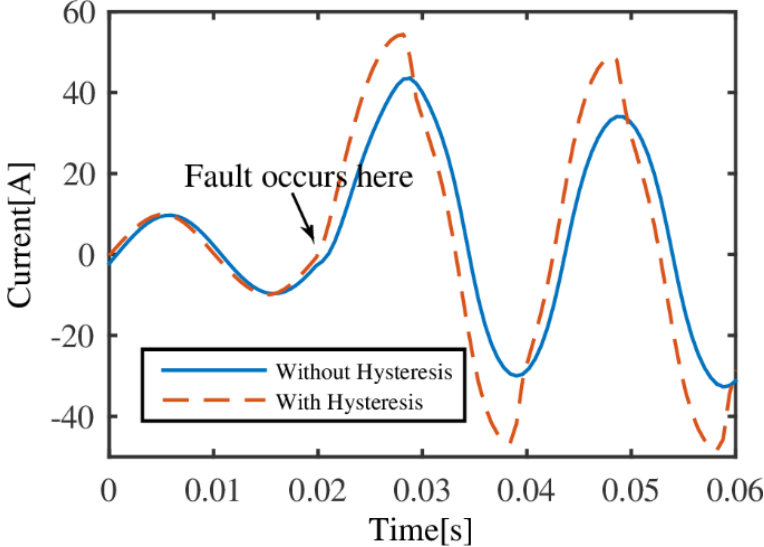


Fig. 2. Comparative plot of circuit current with and without hysteresis

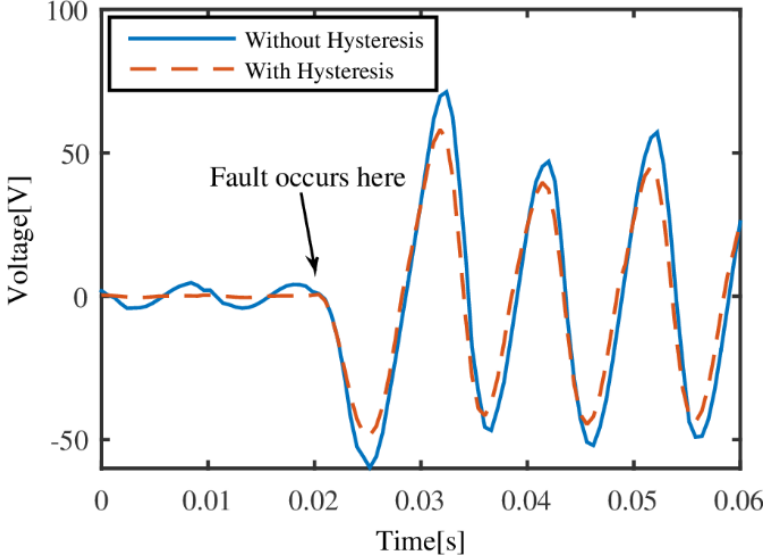


Fig. 3. Comparative plot of voltage across DC coil with and without hysteresis

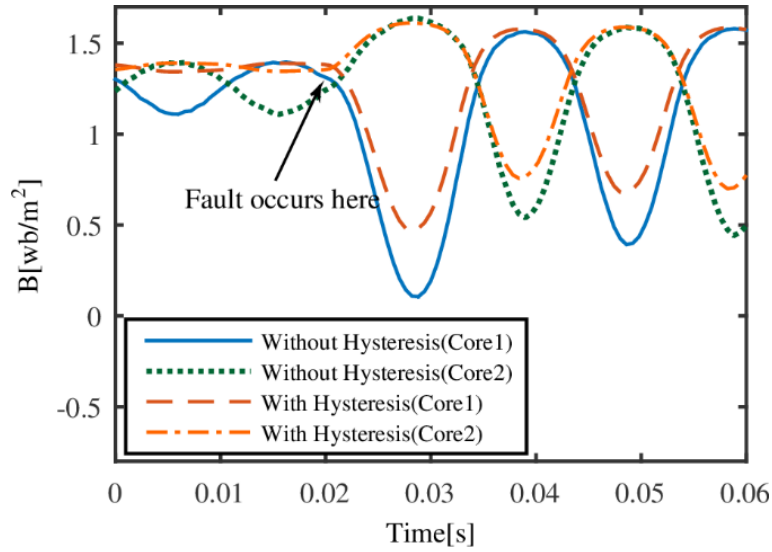


Fig. 4. Comparative plot of flux density across AC coils with and without hysteresis

The same model is simulated neglecting hysteresis. The equivalent B-H curve considered is obtained from the hysteresis model increasing H from zero value without any reversals in direction. The circuit current waveform shown in Fig. 2 illustrates very low impedance offered by the limiter in the normal condition and the increase in impedance during fault. The magnitude of the suppressed fault current is more when in hysteresis is considered than when it is neglected. Moreover there is a small phase lag between two plots. These differences arise as flux density change is much less when the operating point traces the hysteresis loop compared to that for a normal magnetization curve, neglecting hysteresis. The higher change in flux density, in case of a non-hysteretic magnetization curve, gives rise to a comparatively higher inductance in the coil and hence there is a lag in the current waveform. The difference in the waveform will reduce as the operating point of the normal operation moves farther away from the knee flux density. Even in that case of high saturation, the hysteretic effect cannot be totally neglected because in order to limit the fault current, the flux density should reach below the knee flux density and it will decrease at a slower rate if hysteresis is considered. The comparative plot of voltage across DC coil shown in Fig. 3, demonstrate that its magnitude is larger during normal condition neglecting hysteresis. The reason is same as the previous which would be clearer if Fig. 4 is considered. The difference in both magnitude and phase of the current waveform would have been lesser for a core possessing a narrower hysteresis loop. In order to identify the difference, a core with a relatively wider hysteresis loop is taken for analysis.

Table 2. System parameters in the Simulation model

<i>Name</i>	<i>Symbol</i>	<i>Value</i>
Source Voltage	V_s	34V
Source Resistance	R_s	1 m Ω
Source Inductance	L_s	0.033 mH
Resistance(normal condition)	R_n	3.4 Ω
Sum total of Cabling Resistances and the Resistance of the two AC coils	R_1	4.302 m Ω
Resistance(fault condition)	R_f	0.34 Ω
Effective cross-section Area of each limb	A	45.4 cm ²
Mean magnetic path length	l	56 cm
Number of DC windings	w_d	70
Number of AC windings	w_c	20
DC bias current	I_d	15A

6. Simulation results using FEM

Since the change in the magnetic state is essential for the performance of the SISFCL, analysing the model with Finite Element Method (FEM) software becomes crucial. For accurate FEM calculations, it is required to input a precise physical geometry and properties of materials for every part. FEM calculations are carried out with Ansoft Maxwell 2D. The physical model was developed following the data provided in Table 1. Maxwell Transient Solver has been utilized for simulation to analyse the pre-fault and the post-fault state of the proposed SISFCL. The input to the solver was set up such that there is a change in the load resistance value after 0.02s, simulating a faulted condition. The hysteresis data obtained from the J-A hysteresis model using the core parameters, given in Table 1, has been included in the material property of the core. The solver was run for 3 cycles i.e., for a period of 0.06s taking 0.001s as the time step. Fig. 5 shows the flux density distribution in the cores during normal condition where both the cores are observed to be in saturation. On the other hand during fault, shown by Fig. 6, the flux density changes to a lower value to unsaturation whereas the other core moves to a more saturated state.

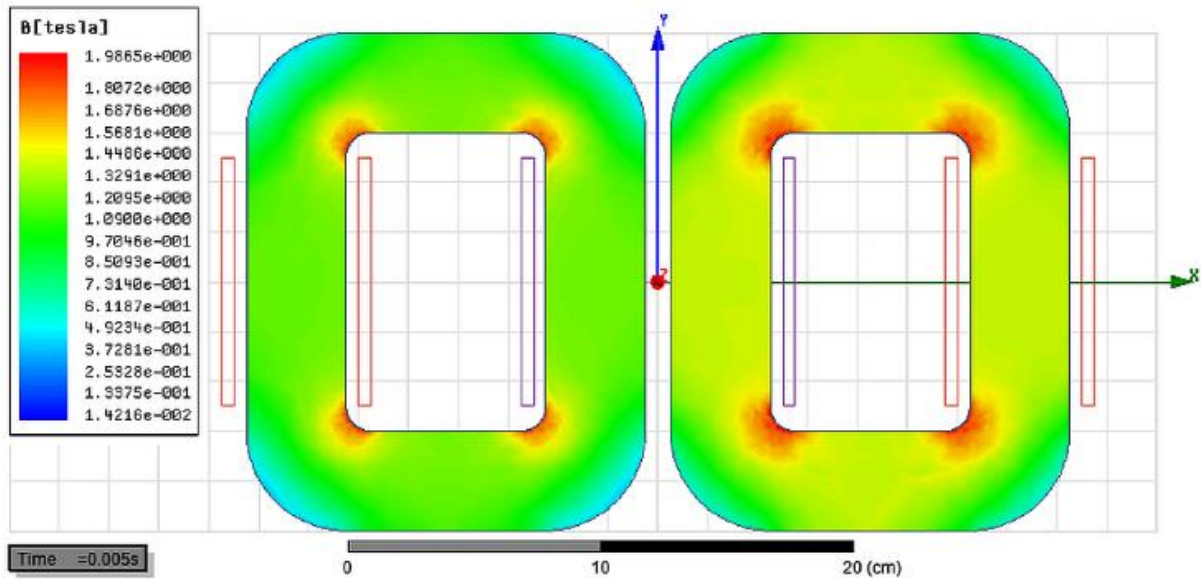


Fig. 5. Flux density distribution in the cores during normal operation

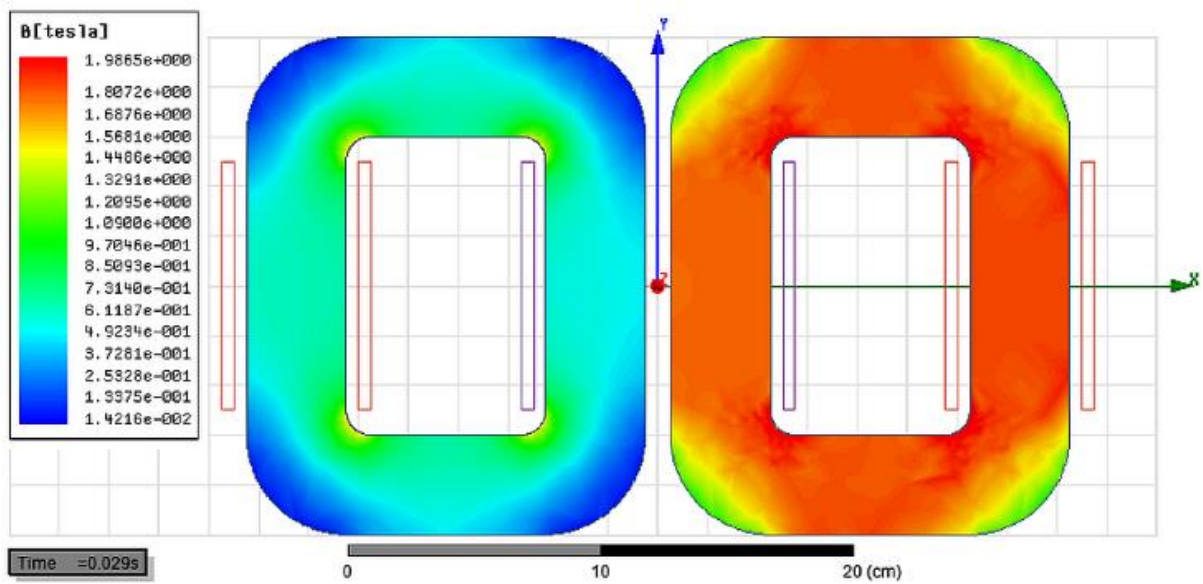


Fig. 6. Flux density distribution in the cores during fault

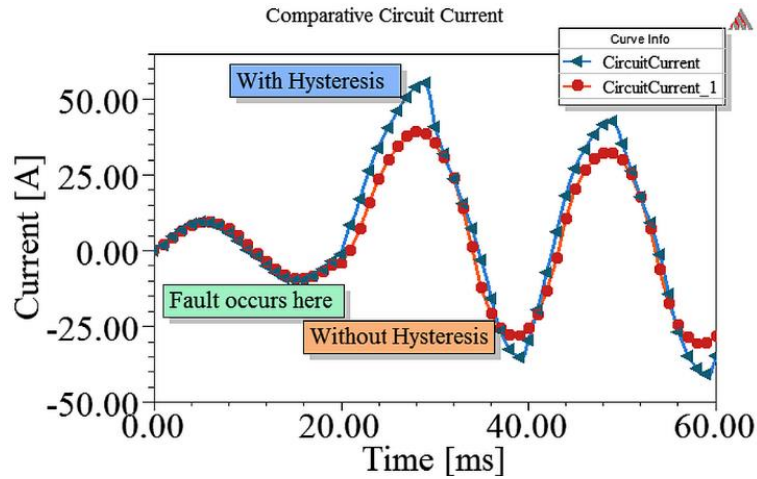


Fig. 7. Comparative plot of circuit current with and without hysteresis obtained from FEM simulation

The transient response of the current waveform obtained from the transient solver is shown in Fig. 7. Fig. 8 shows the comparative plots of voltage across the DC coil. The plot illustrates a good similarity to the plot obtained using MATLAB simulation shown in Fig. 2 and Fig. 3.

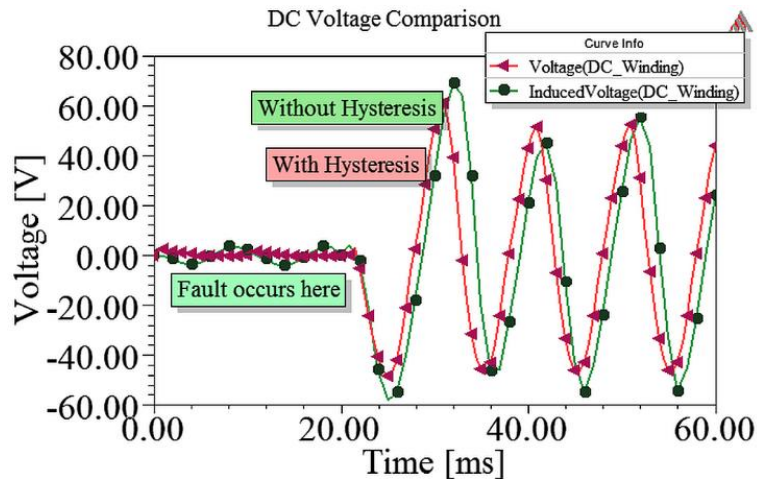


Fig. 8. Comparative plot of voltage across DC coil with and without hysteresis obtained from FEM simulation

7. Harmonic analysis

Most power system device injects unwanted harmonics in the system and SISFCL is no exception. Moreover, the amount of harmonics added is expected to be more when hysteresis is considered. Harmonic analysis of the current waveform for both the cases has been carried out employing both Fast Fourier Transform (FFT) and Continuous Wavelet Transform (CWT).

7.1 Fast Fourier Transform

Analysing signal using FFT is one of the very commonly employed techniques. The current signals obtained from the above simulations are analysed in the MATLAB environment. Since FFT is weak in determining the frequency component and the time instant of its appearance, the current signal is split into two halves showing normal and faulted condition. These two signals are individually analysed.

Fig. 9 describes the comparative FFT plot of circuit current in normal condition considering both hysteresis and the B-H curve. The signal considering hysteresis shows a higher value of harmonics, especially third, fifth and seventh harmonics, with dominating third harmonic [15]. The harmonic content of the faulted signal shown in Fig. 10 again indicates a higher value of harmonics in the signal using hysteresis and the values for third, fifth and seventh harmonic dominate. The signal with hysteresis in faulted condition show a comparatively higher value of fifth harmonic than the normal condition. The presence of the ninth harmonic also becomes noticeable.

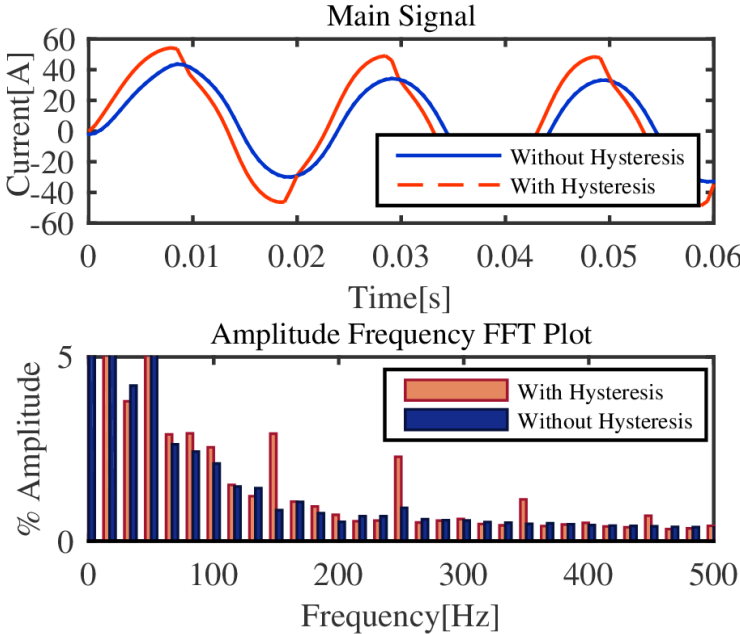


Fig. 9. FFT of circuit current in normal operation

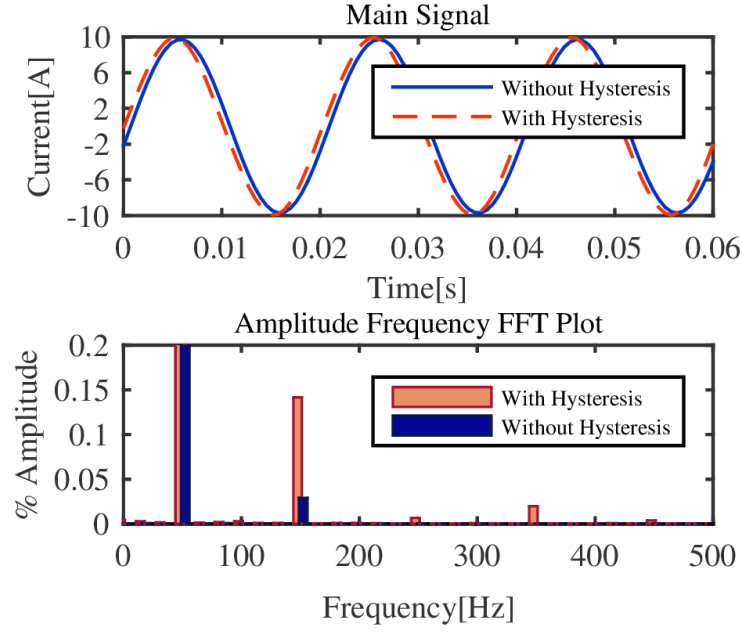


Fig. 10. FFT of circuit current in fault condition

7.2 Continuous Wavelet Transform

Due to spectral leakage, the interharmonic estimation obtained from FFT is erroneous. For accurate time and frequency resolution of the current signal, wavelet transform is the most effective method. In this paper, the Continuous Wavelet Transform (CWT) is used to obtain an accurate time and frequency resolution of a non-stationary signal. For a given signal $f(t)$, the Continuous Wavelet Transform is defined as follows.

$$W(a,b) = \int_t f(t) \frac{1}{\sqrt{|a|}} \Psi^* \left(\frac{t-b}{a} \right) dt \quad (13)$$

And the wavelet is given as,

$$\Psi_{a,b}(t) = \int_t \frac{1}{\sqrt{|a|}} \Psi \left(\frac{t-b}{a} \right) dt \quad (14)$$

$\Psi^*(a,b)$ denotes the complex conjugate of $\Psi(a,b)$. Where a is dilation or scaling parameter and b is translation or location parameter. Wavelet Transform has been performed on the current signal after isolating the normal and faulted signal, as in the case for the FFT analysis. For the following analysis, Morlet wavelet is considered as the mother wavelet. The normal current with

its Continuous Wavelet Transform is shown in Fig. 11. It is clearly visible that the dominant frequency is found to be the fundamental frequency or 50Hz whereas the higher order harmonics are of very low amplitude. The amplitude-frequency plot shows higher amount of harmonics for the signal with hysteresis even under normal condition. Continuous Wavelet Transform of the faulted current signal, shown in Fig. 12, exhibit high harmonic content when hysteretic effect is considered compared to the magnitude of harmonics without hysteresis effect. It may be observed that there is a perceptible presence of third, fifth and seventh order harmonics for the current signal under faulted condition considering the hysteretic effect.

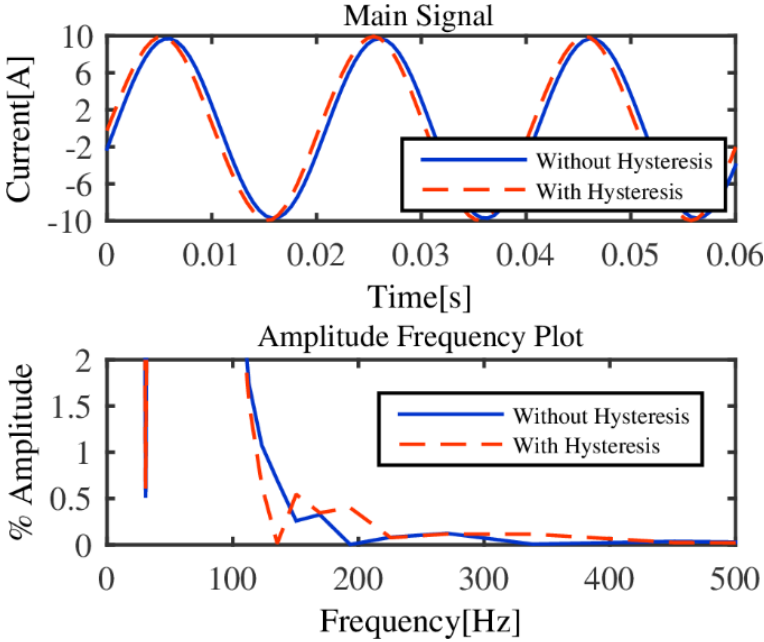


Fig. 11. Wavelet transform of the current signal in normal condition

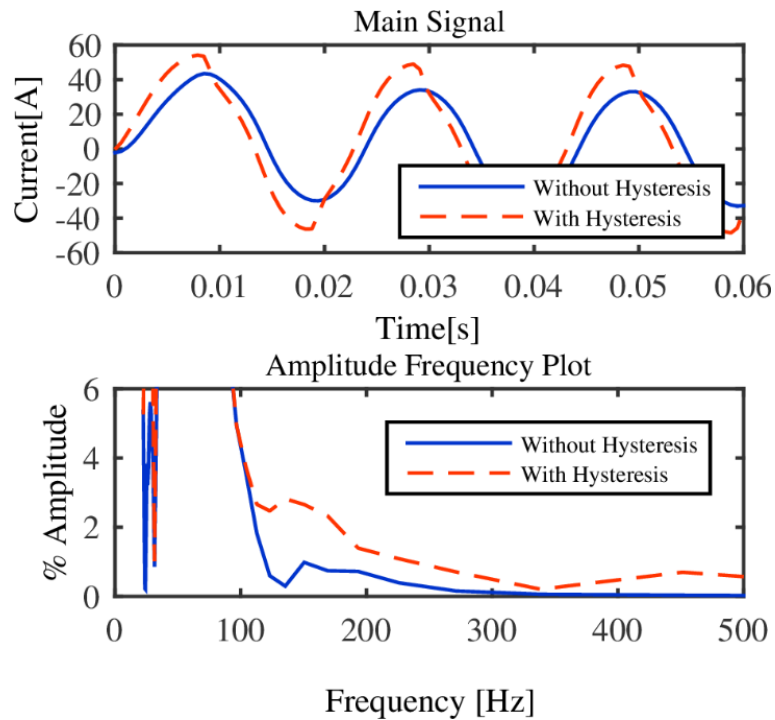


Fig. 12. Wavelet transform of the current signal in fault condition

8. Conclusion

The paper successfully describes the development of the mathematical model of the SISFCL. As the operation of the device depends highly on the change of magnetic state of saturation and unsaturation, inclusion of hysteresis is the accurate approach than using B-H curve for the ferromagnetic cores. The paper presents a novel method of incorporating hysteresis using Jiles Atherton model. The solutions were obtained in MATLAB platform. For comparison, the model is also solved considering B-H curve obtained from the Jiles Atherton model. The comparative plots of both circuit current and the voltage across the DC coil show the error that would be made if B-H curve is used instead of hysteresis. The paper also explained the possible cause of dissimilarity from the comparative plot of flux density in the two cores for both the cases. A core with a comparatively wider hysteresis loop was selected with the operating point closer to the knee flux density so as to provide a more noticeable difference in the performance of SISFCL with and without hysteresis effects. In support of the mathematical model, Finite Element Method is employed using Ansoft Maxwell 2D software. The solution obtained from FEM analysis also supports the validity of the model. Further comparison is made on harmonic aspect of the current signal. Here the signal is divided into normal faulted signal and are separately analysed. Both FFT and CWT (using Morlet wavelet) is performed on the signals. A comparative plot of harmonics contents show relatively high frequency content in the case where hysteresis is

considered. The above discussion successfully presents the importance of considering hysteresis in the SISFCL model.

Acknowledgement

The author sincerely acknowledges the fellowship received from the Department of Science and Technology (DST), Govt. of India under the INSPIRE scheme.

References

1. P. M. Duggan, "Integration issues for fault current limiters and other new technologies - a utility perspective", *IEEE Power Engineering Society General Meeting*, Montreal, Que., pp. 1–3, 2006.
2. P. M. Duggan, "Utility perspective on fault current limiters and expected synergies from integrating fault current limiters with superconducting cables", *IEEE Power and Energy Society General Meeting – Conversion and Delivery of Electrical Energy in the 21st Century*, Pittsburgh, PA, pp. 1–2, 2008.
3. F. Moriconi, F. De La Rosa, A. Singh, B. Chen, M. Levitskaya, A. Nelson, "An innovative compact saturable-core HTS fault current limiter – development, testing and application to transmission class networks", *General meeting of power and energy society, IEEE*, Minneapolis, MN, pp. 1–8, 2010.
4. A. Morandi, "State of the art of superconducting fault current limiters and their application to the electric power system", *Physica C: Superconductivity*, Vol. 484, pp. 242-247, January 2013.
5. Y. Zhang, R.A. Dougal, "State of the art of Fault Current Limiters and their applications in smart grid", *Power and Energy Society General Meeting, 2012 IEEE*, San Diego, CA, pp. 1-6, 22-26 July 2012.
6. S. Kazemia, M. Lehtonen, , Impact of smart subtransmission level fault current mitigation solutions on service reliability, *Electric Power Systems Research*, Vol. 96, pp. 9-15, Mar. 2013.
7. F. Moriconi, F. De La Rosa, F. Darmann, A. Nelson, L. Masur, "Development and deployment of saturated-core fault current limiters in distribution and transmission substations", *IEEE Trans Appl. Supercond.*, vol. 21, pp. 1288-93, 2011.
8. H. Xiao, J. Qiu, S. Wang, Q. Zhang, W. Gong, Y. Xin, J. G. Zhu, Y. Guo, "Analysis of Transient Overvoltage in 220 kV Saturated Core HTS FCL", *Magnetics, IEEE Transactions on*, Vol. 47, No. 10, pp. 2620-2623, Oct. 2011.

9. S.B. Abbott, D.A. Robinson, S. Perera, F.A. Darmann, C.J. Hawley, T.P. Beales, "Simulation of HTS saturable core-type FCLs for MV distribution systems", *Power Delivery, IEEE Transactions on* , vol.21, No.2, pp.1013-1018, April 2006.
10. Y. He, T. Jiang, C.Y. Du, C.B. Li, A.G. Wu, Y. Xin, "Control System Modeling and Simulation of Superconducting Current Limiter With Saturated Iron Core Controlled by DC Bias Current", *Applied Superconductivity, IEEE Transactions on* , vol. 24, No. 5, pp.1-6, Oct. 2014.
11. C. Zhao, S. Wang, J. Qiu, J. G. Zhu, Y. Guo, W. Gong, Z. Cao, "Transient Simulation and Analysis for Saturated Core High Temperature Superconducting Fault Current Limiter", *Electromagnetic Field Computation, 2006 12th Biennial IEEE Conference on* , Miami, FL, vol., No., pp. 503-503, 0-0 0.
12. J.B. Thelke, M.K. Devine, D.C. Jiles, "Numerical determination of hysteresis parameters for the modeling of magnetic properties using the theory of ferromagnetic hysteresis", *IEEE Transactions Magnetics*, vol. 28, pp. 27-35, 1992.
13. J.W. Moscrop, "Experimental Analysis of the Magnetic Flux Characteristics of Saturated Core Fault Current Limiters, Magnetics", *IEEE Transactions on* , vol. 49, No. 2, pp. 874-882, Feb. 2013.
14. J. Cui, Y.W. Sun, H. Hong, X.Y. Niu, B. Tian, Q. Li, J. Y. Zhang, W.Z. Gong, Y. Xin, "Study on Field Suppression Unit in DC Excitation System for Saturated Iron-Core Superconducting Fault Current Limiter", *Applied Superconductivity, IEEE Transactions on* , vol. 24, no. 5, pp.1-4, Oct. 2014.
15. P.A. Commins, J.W. Moscrop, "Three phase saturated core fault current limiter performance with a floating neutral", *Electrical Power and Energy Conference (EPEC), 2012 IEEE* , London, ON, pp. 249-254, 10-12 Oct. 2012.